Kinetics, Kinetic Deuterium Isotope Effects, and Mechanism of Nitrous Oxide Reaction with Hydrogen on Supported Precious-Metal Catalysts

Akira Miyamoto,* Shigeo Baba, Mitsushi Mori, and Yuichi Murakami

Department of Synthetic Chemistry, Faculty of Engineering, Nagoya University, Chikusa-ku, Nagoya 464, Japan
(Received: December 29, 1980; In Final Form: July 6, 1981)

The kinetics and kinetic deuterium isotope effects have been precisely measured for the reaction of nitrous oxide with hydrogen on Ru/Al_2O_3, Rh/Al_2O_3, Ir/Al_2O_3, and Pt/Al_2O_3 catalysts. The reaction apparently proceeds through the two following elementary steps: $N_2O + M \rightarrow N_2 + M{=}O$ (reaction 1) and $M{=}O + H_2 \rightarrow M + H_2O$ (reaction 2). In reaction 1, an N_2O molecule attacks the vacant metal site on the surface (M) to form an N_2 molecule and an adsorbed oxygen atom (M=O). In reaction 2, the reaction of the surface oxygen atom with an H_2 molecule takes place to form an H_2O molecule and the vacant metal site. The activation energy for reaction 1 increases in the order $Ru/Al_2O_3 < Rh/Al_2O_3 < Ir/Al_2O_3 < Pt/Al_2O_3$, whereas for reaction 2 the activation energy decreases in the order $Ru/Al_2O_3 > Rh/Al_2O_3 > Ir/Al_2O_3$. The preexponential factors of the rate constant for both reactions 1 and 2 do not vary significantly from one catalyst to another, although the value for reaction 1 is $\sim 10^4$ times smaller than that for reaction 2. The experimental results have been satisfactorily explained with the transition-state theory coupled with the above-mentioned reaction mechanism.

Introduction

A heterogeneous catalytic reaction is usually composed of two or more elementary reactions.[1-3] It is therefore important for understanding the mechanism of the catalytic reaction (i) to reveal the network of the elementary reactions and (ii) to investigate the rates of the individual elementary reactions in terms of the structures and properties of reactant molecules and the catalyst. Because of the complex nature of heterogeneous catalytic reactions, this has rarely been done even for what are considered to be simple reactions.

The reaction of nitrous oxide with hydrogen ($N_2O + H_2 \rightarrow N_2 + H_2O$, hereafter called the N_2O–H_2 reaction) was the subject of investigations in the very early stage of heterogeneous catalytic chemistry, although definite conclusions were not obtained for the kinetics, kinetic deuterium isotope effects, or the mechanism of the reaction.[4-6] The N_2O–H_2 reaction would, however, be interesting for the investigation of the above-mentioned basic problems in heterogeneous catalytic chemistry, since this reaction is considered to be one of the simplest reactions. In the present study, the kinetics and kinetic deuterium isotope effects of the N_2O–H_2 reaction on supported precious-metal catalysts have been precisely measured and the results discussed in terms of the structures and properties of reactant molecules and catalysts by using the transition-state theory. Supported precious metals were used as catalysts, because investigations of the activities of the catalysts for various types of reactions—including the hydrogenations of carbon monoxide and nitrogen oxides—are highly desirable.[7-10]

Experimental Section

Catalysts and Reagents. Ru/Al_2O_3, Rh/Al_2O_3, Ir/Al_2O_3, and Pt/Al_2O_3 catalysts were prepared by impregnation of γ-Al_2O_3 (Sumitomo Kagaku) with solutions of $RuCl_3 \cdot H_2O$, $RhCl_3 \cdot 3H_2O$, $IrCl_4 \cdot 4H_2O$, and H_2PtCl_6, respectively, followed by drying at 383 K and subsequent reduction in flowing hydrogen at 723 K for Ru/Al_2O_3, Ir/Al_2O_3, and Pt/Al_2O_3, and at 973 K for Rh/Al_2O_3. The content of the precious metal in each catalyst was 0.5 wt %. The surface area of the precious metal on Al_2O_3 was determined by hydrogen-adsorption experiments using a conventional static volumetric apparatus coupled with the number of surface atoms per unit area of polycrystalline surface[11] as follows: 0.28 $m^2\ g^{-1}$ for Ru/Al_2O_3, 1.07 $m^2\ g^{-1}$ for Rh/Al_2O_3, 1.59 $m^2\ g^{-1}$ for Ir/Al_2O_3, and 0.46 $m^2\ g^{-1}$ for Pt/Al_2O_3.

Hydrogen or deuterium was purified by passing it through a Pd/asbestos column and a molecular sieve trap. Helium as a balance gas was purified by passing it through a titanium metal sponge heated at 1073 K and then through a molecular sieve trap. Nitrous oxide (99.8% purity; impurities were 0.06% of N_2 and 0.16% of O_2) was passed through a Pt/Al_2O_3 catalyst bed at room temperature after having been mixed with H_2 (or D_2) and He in order to remove O_2 as an impurity in the N_2O gas. No oxygen was detected by gas chromatography in the mixed gas treated with the Pt/Al_2O_3 catalyst, while the N_2O–H_2 reaction barely took place over the Pt/Al_2O_3 catalyst at room temperature.

Apparatus and Procedure. The kinetics of the N_2O–H_2 or N_2O–D_2 reaction was investigated by using a conventional flow reactor under the following differential reaction conditions: T = 393–473 K; C_{H_2} or C_{D_2} = 0.23–2.27 μmol cm^{-3}; C_{N_2O} = 0.23–2.27 μmol cm^{-3}; W/F = 0.017–0.188 g μmol^{-1} s; total pressure = 101.3 kPa. Particular care was paid to eliminating the heat of the reaction and therefore to the control of reaction temperature. The glass reactor was heated to the reaction temperature by using a fluidized bed, and the catalyst was diluted with α-Al_2O_3.

(1) M. Boudart and R. L. Burwell, Jr., "Investigation of Rates and Mechanisms of Reactions", E. S. Lewis, Ed., Wiley, New York, 1974, Chapter 12.
(2) C. H. Bamford and C. F. H. Tipper, Eds., "Comprehensive Chemical Kinetics", Vol. 20, Elsevier, New York, 1978.
(3) J. Horiuti and T. Nakamura, *Adv. Catal.*, 17, 1 (1967).
(4) J. K. Dixon and J. E. Vance, *J. Am. Chem. Soc.*, 57, 818 (1935).
(5) H. W. Merville, *J. Chem. Soc.*, 797 (1934).
(6) C. N. Hinshelwood, *Proc. R. Soc. London, Ser. A*, 106, 292 (1924).
(7) P. J. Denny and D. A. Whan, "Catalysis", Vol. 2, The Chemical Society, London, 1978, Chapter 3.
(8) M. A. Vannice, *Catal. Rev.*, 14, 153 (1976).
(9) V. Ponec, *Catal. Rev.*, 18, 151 (1978).
(10) M. Shelef, *Catal. Rev.*, 11, 1 (1975).
(11) J. R. Anderson, "Structure of Metallic Catalysts", Academic Press, New York, 1975, Chapter 6.

0022-3654/81/2085-3117$01.25/0

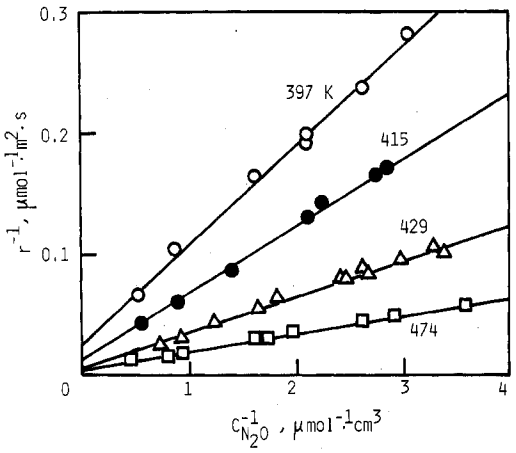

Figure 1. Relationship between r^{-1} and $C_{N_2O}^{-1}$ for the N_2O–H_2 reaction on Ir/Al_2O_3 catalyst at various temperatures. C_{H_2} = 0.96 μmol cm^{-3}.

TABLE I: Arrhenius Parameters for the N_2O–H_2 Reaction on Ru/Al_2O_3, Rh/Al_2O_3, Ir/Al_2O_3, and Pt/Al_2O_3

catalyst	A_1, cm s^{-1}	A_2, cm s^{-1}	E_1, kJ mol^{-1}	E_2, kJ mol^{-1}
Ru/Al_2O_3	1.97	1.43 × 10^4	21.4	59.9
Rh/Al_2O_3	2.94	1.57 × 10^4	21.5	52.7
Ir/Al_2O_3	4.61	1.62 × 10^4	26.5	49.4
Pt/Al_2O_3	2.42		36.4	

Results

Kinetics of the N_2O–H_2 Reaction. Before proceeding with the kinetic experiments, we confirmed that neither γ-Al_2O_3 as the support of the precious metal nor α-Al_2O_3 as the diluent of the catalysts showed activity for the N_2O–H_2 reaction. The H_2O produced by the reaction was also shown to exert no effect on the reaction rate, provided the reaction temperature was higher than 383 K.

The rate of the N_2O–H_2 reaction was measured under various experimental conditions, namely, at various temperatures and at various concentrations of N_2O and H_2. In this study, the reaction rate (denoted by r) is expressed as the specific rate defined by the rate of the formation of N_2 divided by the surface area of the precious metal. For all catalysts, the observed rates were most consistent with eq II, which is identical with eq I, although various other types of rate equations were also compared to the experimental data.

$$r = k_1k_2C_{N_2O}C_{H_2}(k_1C_{N_2O} + k_2C_{H_2})^{-1} \quad \text{(I)}$$

$$r^{-1} = (k_1C_{N_2O})^{-1} + (k_2C_{H_2})^{-1} \quad \text{(II)}$$

Figure 1 shows examples of the observed relationships between r^{-1} and $C_{N_2O}^{-1}$ for the Ir/Al_2O_3 catalyst. Consistent with eq II, a linear relationship was observed between r^{-1} and $C_{N_2O}^{-1}$ at any temperature indicated. Similarly, a linear relationship between r^{-1} and $C_{H_2}^{-1}$ was found for the N_2O–H_2 reaction on Ir/Al_2O_3, and the rate constants, k_1 and k_2, were approximately equal to those determined from a linear plot of r^{-1} vs. $C_{N_2O}^{-1}$, as shown in Figure 2. Figure 2 shows the temperature dependence of the observed rate constants which satisfy the Arrhenius equations:

$$k_1 = A_1 \exp(-E_1/RT) \quad \text{(III)}$$

$$k_2 = A_2 \exp(-E_2/RT) \quad \text{(IV)}$$

The Arrhenius parameters for the N_2O–H_2 reaction on all of the catalysts are shown in Table I. It should be noted that under the present experimental conditions the rate of the N_2O–H_2 reaction on Pt/Al_2O_3 was first order and zeroth order with respect to C_{N_2O} and C_{H_2}, respectively. Since such dependence of the rate on C_{N_2O} and C_{H_2} can be

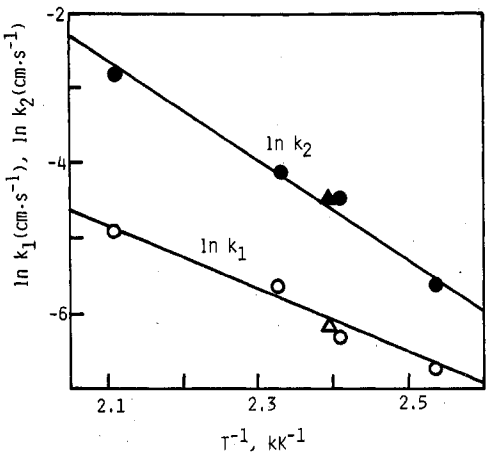

Figure 2. Arrhenius plots of the rate constants, k_1 and k_2, for the N_2O–H_2 reaction on Ir/Al_2O_3 catalyst. Open and closed circles: Rate constants determined from the relationships between r^{-1} and $C_{N_2O}^{-1}$. Open and closed triangles: Rate constants determined from the relationship between r^{-1} and $C_{H_2}^{-1}$.

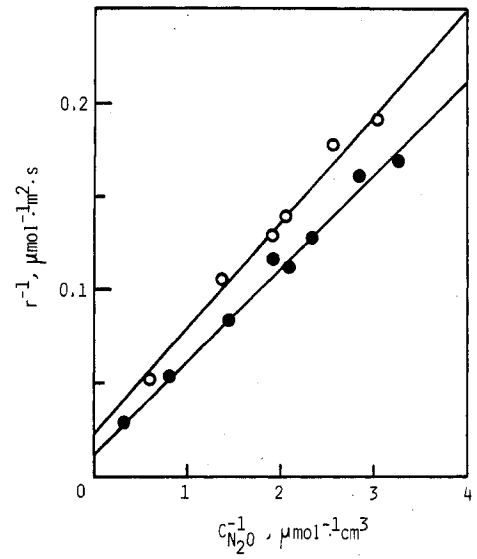

Figure 3. Relationship between r^{-1} and $C_{N_2O}^{-1}$ for the N_2O–H_2 reaction (closed circles) and that for the N_2O–D_2 reaction (open circles) on Ir/Al_2O_3 catalyst. C_{H_2} = 0.97 μmol cm^{-3}. C_{D_2} = 1.00 μmol cm^{-3}. Reaction temperature = 415 K.

expected for the special case where $k_1C_{N_2O}$ is significantly smaller than $k_2C_{H_2}$ in eq I or II, the kinetic treatment described above can be applied to the N_2O–H_2 reaction on Pt/Al_2O_3 catalyst. In other words, concerning the N_2O–H_2 reaction on Pt/Al_2O_3, only A_1 and E_1 for k_1 were determined from the measured kinetics of the reaction.

Kinetic Deuterium Isotope Effect. The rate of the reaction of N_2O with D_2 (the N_2O–D_2 reaction) was measured under the same experimental conditions as those for the N_2O–H_2 reaction. Figure 3 shows the relationship between r^{-1} and $C_{N_2O}^{-1}$ for the N_2O–D_2 reaction and that for the N_2O–H_2 reaction on the Ir/Al_2O_3 catalyst. From these relationships, k_1 and k_2 for the N_2O–H_2 reaction—k_1^H and k_2^H—and those for the N_2O–D_2 reaction—k_1^D and k_2^D—were determined. The results are indicated in Table II as the values of the kinetic deuterium isotope effects, that is, k_1^H/k_1^D and k_2^H/k_2^D. From the relationship between r^{-1} and $C_{H_2}^{-1}$ and that between r^{-1} and $C_{D_2}^{-1}$ shown in Figure 4, k_1^H/k_1^D and k_2^H/k_2^D were also determined. These results are also shown in Table II. In the same way, the kinetic isotope effects were also determined for the reaction on Ru/Al_2O_3, Rh/Al_2O_3, and Pt/Al_2O_3 (Table II). As

TABLE II: Kinetic Isotope Effects in k_1 and k_2 for the N_2O–H_2 Reaction on Ru/Al_2O_3, Rh/Al_2O_3, Ir/Al_2O_3, and Pt/Al_2O_3

	Ru/Al_2O_3			Rh/Al_2O_3			Ir/Al_2O_3			
	A^a	B^b	av^c	A^a	B^b	av^c	A^a	B^b	av^c	Pt/Al_2O_3 A^a
k_1^H/k_1^D	1.03	0.97	1.00	0.90	1.01	0.96	1.13	0.95	1.04	1.00
k_2^H/k_2^D	1.64	1.66	1.65	1.80	1.51	1.67	2.09	1.75	1.92	

[a] Kinetic isotope effects determined by the relationship between r^{-1} and $C_{N_2O}^{-1}$. [b] Kinetic isotope effects determined by the relationship between r^{-1} and $C_{H_2}^{-1}$ (or $C_{D_2}^{-1}$). [c] Average of A and B.

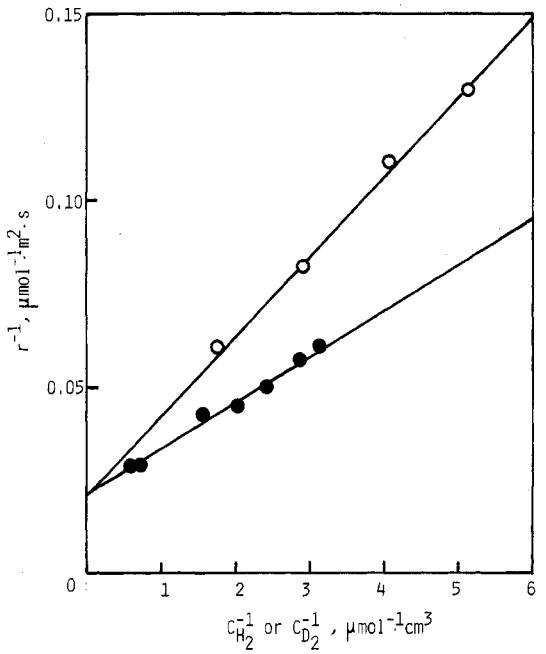

Figure 4. Relationship between r^{-1} and $C_{H_2}^{-1}$ for the N_2O–H_2 reaction (closed circles) and that between r^{-1} and $C_{D_2}^{-1}$ for the N_2O–D_2 reaction (open circles). C_{N_2O} = 2.31 μmol cm^{-3}. Reaction temperature = 415 K.

shown in Table II, a significant kinetic deuterium isotope effect appeared in k_2, whereas no kinetic isotope effect appeared in k_1 for all catalysts employed.

Discussion

Mechanism of the N_2O–H_2 Reaction. On the basis of the measured kinetics of the N_2O–H_2 reaction coupled with the data of the kinetic deuterium isotope effects, a mechanism shown in Figure 5 can be proposed for the N_2O–H_2 reaction on Ru/Al_2O_3, Rh/Al_2O_3, Ir/Al_2O_3, and Pt/Al_2O_3. According to this mechanism, first, an N_2O molecule attacks a vacant metal site (reaction 1) to form an N_2 molecule and an adsorbed oxygen atom (M=O); k_1 is the rate constant for this step. Then, an H_2 molecule attacks the M=O species to form an H_2O molecule and a vacant metal site (reaction 2); k_2 is the rate constant for reaction 2. This mechanism coupled with the assumption of the steady-state reaction condition readily leads to eq I or II, which satisfies the experimental kinetics under steady-state conditions. The data of the kinetic isotope effects (Table II) are consistent with the mechanism but rule out an alternative mechanism where an N_2O molecule attacks adsorbed hydrogen atoms on the catalyst. If the latter mechanism played an essential role in the N_2O–H_2 reaction, a significant kinetic isotope effect should appear in k_1, which is in contradiction to the experimental kinetic isotope effects (Table II). According to the mechanism shown in Figure 5, the kinetic isotope effect cannot appear in k_1 but should appear in k_2. This agrees with the experimental data shown in Table II. It should also be noted in Table II that the value of the kinetic isotope effect in

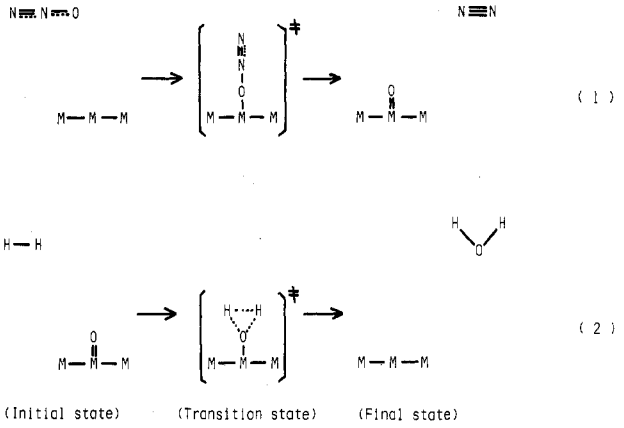

Figure 5. Mechanism of the N_2O–H_2 reaction.

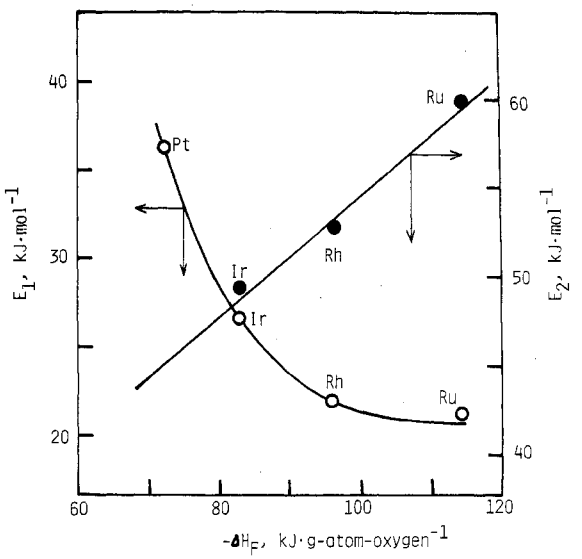

Figure 6. Relationships between the activation energies for the rate constants (E_1 and E_2) and the heat of formation of metal oxide (ΔH_F).

k_2 is almost constant for all catalysts employed. Since the value of the kinetic isotope effect reflects the structure of the transition state of a reaction, this means that the structure of the transition state of reaction 2 is almost the same for all catalysts.

Effects of the Kind of Precious Metal on the Mechanism of the N_2O–H_2 Reaction. Figure 6 shows the relationship between the activation energies and the heat of formation of metal oxide (ΔH_F). Here, ΔH_F is defined as the enthalpy change for the oxidation of Ru, Rh, Ir, or Pt metal to RuO_2, Rh_2O, IrO_2, or PtO, which is reported to be the metal oxide with the lowest oxidation state for each precious metal, divided by the number of oxygen atoms of the metal oxide.[12,13] As shown in Figure 6, E_1 decreases as the absolute value of ΔH_F ($|\Delta H_F| = -\Delta H_F$) increases,

(12) R. C. Weast, Ed., "Handbook of Chemistry and Physics", Chemical Rubber Publishing Co., Cleveland, OH, 1970, p D45.
(13) G. B. Samsonov, Ed., "Physico-Chemical Properties of Oxides", Moscow, 1969, Chapter 2.

TABLE III: Calculated A_1 and A_2 for the N_2O–H_2 Reaction on Ru/Al_2O_3, Rh/Al_2O_3, Ir/Al_2O_3, and Pt/Al_2O_3[a]

catalyst	ρ, Å	A_1, cm s^{-1}	A_2, cm s^{-1}
Ru/Al_2O_3	1.32	1.64	1.00×10^4
Rh/Al_2O_3	1.34	1.70	1.00×10^4
Ir/Al_2O_3	1.35	1.73	1.00×10^4
Pt/Al_2O_3	1.38	1.80	

[a] Temperature = 423 K. ρ is the radius of metal atom (cf. Figure 7a).

while E_2 increases as $|\Delta H_F|$ increases. Since $|\Delta H_F|$ is considered to be a mesure of the metal–oxygen bond energy,[14] the data shown in Figure 6 demonstrate the following relationship: as the metal–oxygen bond energy increases, E_1 becomes smaller while E_2 becomes larger. This is in accordance with the mechanism of the N_2O–H_2 reaction shown in Figure 5. When an N_2O molecule attacks a vacant metal site to form an N_2 molecule and an adsorbed oxygen atom (reaction 1), the activation energy (E_1) should be lower on a catalyst with a stronger metal–oxygen bond. When an H_2 molecule attacks the adsorbed oxygen atom to form an H_2O molecule and a vacant metal site (reaction 2), in the opposite way, the activation energy (E_2) should be larger on a catalyst with a stronger metal–oxygen bond.

Analysis of the Rate Constants Using the Transition-State Theory. According to the transition-state theory,[15,16] rate constants, especially preexponential factors, are a sensitive reflection of details of reaction mechanisms. As shown in Table I, neither A_1 nor A_2 varies significantly with the kind of precious metal. The value of A_2 is ca. 10^4 times larger than A_1 for all catalysts. In order to prove the validity of the mechanism shown in Figure 5, one should satisfactorily interpret these facts in terms of the transition-state theory.

According to the transition-state theory applied to the reaction mechanism shown in Figure 5, the rate constants for the N_2O–H_2 reaction can be formulated as follows:

$$k_1 = L\frac{k_BT}{h}\frac{1}{(2\pi m_{N_2O}k_BT)^{1/2}/h}\frac{f^*_{rot}f^*_{vib}}{f^{rot}_{N_2O}f^{vib}_{N_2O}f_s}s_1\exp(-\epsilon_1/k_BT) \quad (V)$$

$$k_2 = L\frac{k_BT}{h}\frac{1}{(2\pi m_{H_2}k_BT)^{1/2}/h}\frac{f^*_{rot}f^*_{vib}}{f^{rot}_{H_2}f^{vib}_{H_2}f_o}s_2\exp(-\epsilon_2/k_BT) \quad (VI)$$

where s_1 and s_2 are areas of the active sites for reactions 1 and 2, respectively. Judging from the structures of the transition states for reactions 1 and 2 shown in Figure 5, the values of the rotational and vibrational partition functions for the transition states, that is, the values of f^*_{rot} and f^*_{vib} are considered to be 1. Similarly, the values of the partition function for the vacant metal site, f_s, and that of the surface oxygen, f_o, can be considered to be 1. Equations V and VI then lead to eq VII and VIII, respectively. Preexponential factors for k_1 and k_2 can therefore be given by eq IX and X. In order to calculate

$$k_1 = L\left(\frac{k_BT}{2\pi m_{N_2O}}\right)^{1/2}\frac{s_1}{f^{rot}_{N_2O}}\exp(-\epsilon_1/k_BT) \quad (VII)$$

$$k_2 = L\left(\frac{k_BT}{2\pi m_{H_2}}\right)^{1/2}\frac{s^2}{f^{rot}_{H_2}}\exp(-\epsilon_2/k_BT) \quad (VIII)$$

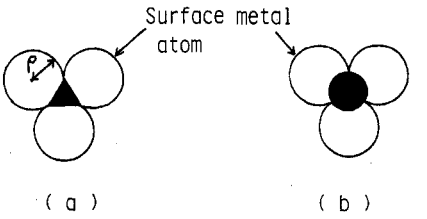

Figure 7. Areas of the active sites for reactions 1 and 2: (a) s_1 for reaction 1; $s_1 = \sqrt{3}\rho^2/4$, where ρ is the radius of metal atom. (b) s_2 for reaction 2; $s_2 = 2\pi\rho_o^2$, where ρ_o is the radius of adsorbed oxygen atom.

$$A_1 = L\left(\frac{k_BT}{2\pi m_{N_2O}}\right)^{1/2}\frac{s_1}{f^{rot}_{N_2O}} \quad (IX)$$

$$A_2 = L\left(\frac{k_BT}{2\pi m_{H_2}}\right)^{1/2}\frac{s_2}{f^{rot}_{H_2}} \quad (X)$$

A_1 and A_2, one should evaluate the values of s_1 and s_2. s_2 was estimated to be the area of a hemisphere of the adsorbed oxygen atom (cf. Figure 7b); its radius was that of the single bond of an oxygen atom (ρ_o = 0.74 Å).[17] The s_1 was tentatively assumed to be the area covered by the shaded triangle at the e_g or t_{2g} site on a (010) plane of fccub crystal (cf. Figure 7a). Since the value of L can be found,[11] A_1 and A_2 can be calculated for any metal. From the results shown in Table III, the calculated A_1 and A_2 values agree with the experimental values shown in Table I. The method of estimating s_1 shown in Figure 7a is not unique; therefore, the calculated value of A_1 can change with the estimated value of s_1. However, the magnitude of change in A_1 is not significant. This is because calculated A_1 is at most 8 times larger than the experimental A_1, even if the entire metal surface serves as the active site for reaction 1. These data indicate the validity of the mechanism shown in Figure 5. It should also be emphasized that the calculated A_2 is ca. 10^4 times greater than the calculated A_1, in accordance with the experimental relationship between A_1 and A_2. According to eq IX and X, this difference is due to the difference in the molecular weight between N_2O and H_2, which causes the difference in the translational and rotational partition functions.

It is well-known that a gaseous H_2 can readily dissociate on a precious metal to form adsorbed hydrogen atoms. According to the mechanism shown in Figure 5, however, the adsorbed hydrogen atoms do not play a significant role in the N_2O–H_2 reaction. It is therefore considered that the reaction of the adsorbed oxygen atom with the adsorbed hydrogen atoms proceeds more slowly than reaction 2 in Figure 5. This agrees with the mechanism proposed by Weinberg et al. based on the BEBO method,[18] which indicates that an adsorbed oxygen atom on Pt(111) surface can react more readily with a gaseous H_2 than with adsorbed hydrogen atoms. It should also be noted that the effect of the adsorbed hydrogen atoms is not taken into consideration in eq I or II. Since the hydrogen atom is much smaller than the surface metal atom or adsorbed oxygen atom, this may be because the kinetics of reaction 1 or 2 is not much affected by the presence of the adsorbed hydrogen atom.

(14) K. van der Wiele and P. J. van der Berg, "Comprehensive Chemical Kinetics", Vol. 20, Elsevier, New York, 1978, Chapter 2.
(15) K. J. Laidler, "Catalysis", P. H. Emmett, Ed., Vol 1, Reinhold, New York, 1954, Chapter 5.
(16) S. Glasstone, K. J. Laidler, and H. Eyring, "The Theory of Rate Processes", McGraw-Hill, New York, 1964, Chapter 7.
(17) L. Pauling, "Nature of Chemical Bonds", Cornell University Press, New York, 1960, Chapter 7.
(18) W. H. Weinberg and R. P. Merrill, *J. Catal.*, **40**, 268 (1975).

TABLE IV: Kinetic Isotope Effect and Vibrational Frequency for the Activated Complex of Reaction 2

	k_2^H/k_2^D		$[\omega_a(H\cdots O\cdots H) + \omega_2(H\cdots O\cdots H + H\cdots H)]$, cm^{-1}	
catalyst	exptl	calcd	exptl	calcd
Ru/Al_2O_3	1.65	1.72	5437	5373
Rh/Al_2O_3	1.67	1.72	5413	5373
Ir/Al_2O_3	1.92	1.72	5133	5373

Analysis of the Kinetic Isotope Effect with the Transition-State Theory and the BEBO Method. On the basis of eq VIII, the kinetic isotope effect for k_2 can be given by eq XI. Here, $(m_{D_2}/m_{H_2})^{1/2}$, $f_{D_2}^{rot}/f_{H_2}^{rot}$, and $(\epsilon_2^D - \epsilon_2^H)/k_BT$

$$k_2^H/k_2^D = \left(\frac{m_{D_2}}{m_{H_2}}\right)^{1/2}\left(\frac{f_{D_2}^{rot}}{f_{H_2}^{rot}}\right)\exp[(\epsilon_2^D - \epsilon_2^H)/k_BT] \quad (XI)$$

are kinetic isotope effects due to the translational partition function (or the collision frequency), the rotational partition function, and the activation energy, respectively. The values of $(m_{D_2}/m_{H_2})^{1/2}$ and $f_{D_2}^{rot}/f_{H_2}^{rot}$ can easily be calculated, and eq XI then leads to eq XII. According to the

$$k_2^H/k_2^D = 2^{3/2}\exp[(\epsilon_2^D - \epsilon_2^H)/k_BT] \quad (XII)$$

theory of the kinetic deuterium isotope effect,[19,20] $\epsilon_2^D - \epsilon_2^H$ is the zero-point energy difference for the vibrations where H or D atoms are involved. For reaction 2, such vibrational modes are mainly H–H (or D–D) stretching vibration, ν(H–H) (or ν(D–D)), for the initial state, and H···O···H (or D···O···D) asymmetric vibration, ν_a(H···O···H) (or ν_a(D···O···D)), and two coupled vibrations between H···H (or D···D) stretching vibration and H···O···H (or D···O···D) symmetric vibration, ν_1(H···O···H + H···H) (or ν_1(D···O···D + D···D)) and ν_2(H···O···H + H···H) (or ν_2(D···O···D + D···D)), for the transition state. Here, one of the coupled vibrations, ν_1(H···O···H + H···H), is parallel to the reaction coordinate, and the other, ν_2(H···O···H + H···H), is perpendicular to the reaction coordinate. Since the vibrational mode parallel to the reaction coordinate does not contribute to the zero-point energy at the transition state, $\epsilon_2^D - \epsilon_2^H$ is given by

$$\epsilon_2^D - \epsilon_2^H = (hc/2)[\{\omega_a(D\cdots O\cdots D) + \omega_2(D\cdots O\cdots D + D\cdots D) - \omega(D\text{–}D)\} - \{\omega_a(H\cdots O\cdots H) + \omega_2(H\cdots O\cdots H + H\cdots H) - \omega(H\text{–}H)\}] \quad (XIII)$$

The following relationships hold approximately for the wavenumber of vibrations involving H or D atoms:[19]

$$\omega_a(D\cdots O\cdots D) = \omega_a(H\cdots O\cdots H)/\sqrt{2} \quad (XIV)$$

$$\omega_2(D\cdots O\cdots D + D\cdots D) = \omega_2(H\cdots O\cdots H + H\cdots H)/\sqrt{2} \quad (XV)$$

Equation XIII then leads to eq XVI. On the basis of eq

$$\epsilon_2^D - \epsilon_2^H = (hc/2)[\{\omega(H\text{–}H) - \omega(D\text{–}D)\} - (1 - 1/\sqrt{2}) \times \{\omega_a(H\cdots O\cdots H) + \omega_2(H\cdots O\cdots H + H\cdots H)\}] \quad (XVI)$$

XII and XVI coupled with the measured wavenumber for ν(H–H) (ω(H–H) = 4395 cm^{-1}) and ν(D–D) (ω(D–D) = 3119 cm^{-1}), $\omega_a(H\cdots O\cdots H) + \omega_2(H\cdots O\cdots H + H\cdots H)$ can be calculated for each precious metal from the observed value of k_2^H/k_2^D. The results are shown in Table IV. This table indicates that considerable vibrational frequencies are left in the transition state.

In order to prove the validity of the mechanism shown in Figure 5, one should estimate the value of $\omega_a(H\cdots O\cdots H) + \omega_2(H\cdots O\cdots H + H\cdots H)$ theoretically. The most precise way to estimate $\omega_a(H\cdots O\cdots H) + \omega_2(H\cdots O\cdots H + H\cdots H)$ is to calculate the exact potential energy surface near the transition state. Unfortunately, such a detailed method has not been established for reactions on a solid metal catalyst. In the present study, as a first approximation, the BEBO method[21] was applied to evaluate roughly the vibrational frequencies for the activation complex. The bond orders of the individual bonds for the initial state of reaction 2 are as follows: n(H–H) = 1, n(H–O) = 0, and n(M–O) = 2, since the initial state of reaction 2 is composed of a gaseous H_2 and an adsorbed oxygen atom. On the other hand, the final state of reaction 2 is composed of a gaseous H_2O and a vacant surface metal site. Therefore, the bond orders for the final state are as follows: n(H–H) = 0, n(H–O) = 1, and n(M–O) = 0. Assuming that the bond orders for the transition state are calculated by using the mean values of the initial state and the final state, we get the following relationships for the bond orders of the activated complex: n(H–H) = $^1/_2$, n(H–O) = 1/2, and n(M–O) = 1. According to the BEBO method, the force constant for a special bond is proportional to its bond order.[21] Therefore, the wavenumber of the stretching vibration of the H···H bond defined by ω(H···H), and that of the O···H bond defined by ω(O···H) for the activated complex, can be given by eq XVII and XVIII, respectively.

$$\omega(H\cdots H) = \omega(H\text{–}H)(n(H\text{–}H))^{1/2} = 4395/\sqrt{2} = 3108\ cm^{-1} \quad (XVII)$$

$$\omega(O\cdots H) = \omega(O\text{–}H)(n(O\text{–}H))^{1/2} = 3600/\sqrt{2} = 2546\ cm^{-1} \quad (XVIII)$$

Here, standard values of ω(H–H) and ω(O–H) are substituted in order to estimate ω(H···H) and ω(O···H). Since the wavenumber of the symmetric vibration of H_2O is approximately equal to that of the O–H single bond, the following relationship would similarly hold between ω_a(H···O···H) and ω(O···H) for the activated complex:

$$\omega_a(H\cdots O\cdots H) = \omega(O\cdots H) = 2546\ cm^{-1} \quad (XIX)$$

The method for estimating the wavenumber of the coupled vibration between the symmetric H···O···H stretching vibration and the H···H stretching vibration from ω(H···H) and ω(O···H) has not been established. However, the following relationship would provide a close approximation:

$$\omega_2(H\cdots H + H\cdots H) = [\omega(O\cdots H) + \omega(H\cdots H)]/2 = 2327\ cm^{-1} \quad (XX)$$

Therefore, the sum of the wavenumber for the activated complex of reaction 2 can be given by eq XXI on the basis

$$\omega_a(H\cdots O\cdots H) + \omega_2(H\cdots O\cdots H + H\cdots H) = 5373\ cm^{-1} \quad (XXI)$$

of eq XIX and XX. This value agrees with the experimental one shown in Table IV. From the estimated value of $\omega_a(H\cdots O\cdots H) + \omega_2(H\cdots O\cdots H + H\cdots H)$ shown in eq XXI coupled with eq XII and XVI a theoretical value of k_2^H/k_2^D can be calculated. This is also shown in Table IV. As shown, the calculated isotope effect agrees with the

(19) A. Ozaki, "Isotopic Studies of Heterogeneous Catalysis", Kodansha, Tokyo, 1977, Chapter 6.
(20) L. Melander, "Isotope Effect on Reaction Rates", Ronald Press, New York, 1960.
(21) H. S. Johnston, "Gas Phase Reaction Rate Theory", Ronald Press, New York, 1966.

experimental results. Consequently, the kinetic deuterium isotope effect observed for k_2 has been successfully explained in terms of the reaction mechanism shown in Figure 5, indicating the validity of the mechanism.

Acknowledgment. We are grateful to Professor A. Ozaki for his continuing interest and encouragement. This work was partially supported by a Grant-in-Aid for Encouragement of Young Scientists from the Ministry of Education, Japan (No. 375451).

Glossary

C_{H_2}, C_{D_2}	concentration of H_2 or D_2 in the gas phase, mol cm^{-3} or molecules cm^{-3}
C_{N_2O}	concentration of N_2O in the gas phase, mol cm^{-3} or molecules cm^{-3}
r	specific rate of the N_2O–H_2 or N_2O–D_2 reaction, mol cm^{-2} s^{-1} or molecules cm^{-2} s^{-1}
k_1, k_2	rate constant, cm s^{-1}
A_1, A_2	preexponential factor, cm s^{-1}
E_1, E_2	activation energy, J mol^{-1}
ϵ_1, ϵ_2	activation energy, erg
T	temperature, K
R	gas constant, J K^{-1} mol^{-1}
ΔH_F	enthalpy change for the oxidation of precious metal, J (g-atom of oxygen)$^{-1}$
L	number of sites per unit metal surface area, sites cm^{-2}
s_1, s_2	area of the active site, cm^2
k_B	Boltzmann's constant, erg K^{-1}
h	Planck's constant, erg s
m_{H_2}, m_{D_2}	weight of H_2 or D_2 molecule, g
m_{N_2O}	weight of N_2O molecule, g
f^*_{rot}	rotational partition function for the activated complex, dimensionless
f^*_{vib}	vibrational partition function for the activated complex, dimensionless
$f^{rot}_{N_2O}$	rotational partition function for the N_2O molecule in the gas phase, dimensionless
$f^{vib}_{N_2O}$	vibrational partition function for the N_2O molecule in the gas phase, dimensionless
$f^{rot}_{H_2}$, $f^{rot}_{D_2}$	rotational partition function for the H_2 or D_2 molecule in the gas phase, dimensionless
$f^{vib}_{H_2}$, $f^{vib}_{D_2}$	vibrational partition function for the H_2 or D_2 molecule in the gas phase, dimensionless
f_s	partition function for the vacant metal site, site^{-1}
f_o	partition function of the surface oxygen, site^{-1}
ϵ_1^H, ϵ_2^H	ϵ_1 or ϵ_2 for the N_2O–H_2 reaction, erg
ϵ_1^D, ϵ_2^D	ϵ_1 or ϵ_2 for the N_2O–D_2 reaction, erg
k_1^H, k_2^H	k_1 or k_2 for the N_2O–H_2 reaction, cm s^{-1}
k_1^D, k_2^D	k_1 or k_2 for the N_2O–D_2 reaction, cm s^{-1}
ω_a(H···O···H), ω_a(D···O···D)	wavenumber for the H···O···H or D···O···D asymmetric stretching vibration for the activated complex of reaction 2, cm^{-1}
ω_2(H···O···H + H···H), ω_2(D···O···D + D···D)	wavenumber for the coupled vibration between H···H (or D···D) stretching vibration and H···O···H (or D···O···D) symmetric stretching vibration for the activated complex of reaction 2, cm^{-1}
ω(H–H), ω(D–D)	wavenumber for the H–H (or D–D) stretching vibration of H_2 (or D_2) molecule in the gas phase, cm^{-1}
n(H–H)	bond order of H–H bond, dimensionless
n(H–O)	bond order of H–O bond, dimensionless
n(M–O)	bond order of M–O bond, dimensionless
ω(O–H)	wavenumber for the stretching vibration of O–H single bond, cm^{-1}
ω(O···H)	wavenumber for the stretching vibration of O···H bond for the activated complex, cm^{-1}
ω(H···H)	wavenumber for the stretching vibration of H···H bond for the activated complex, cm^{-1}

Kinetic Study of a Photogalvanic Effect in the $Ru(bpy)_3^{2+}$–Benzenethiolate Anion System

Tokuji Miyashita and Minoru Matsuda*

Chemical Research Institute of Nonaqueous Solutions, Tohoku University, Katahira 2-1-1, Sendai, 980 Japan *(Received: March 9, 1981; In Final Form: July 7, 1981)*

The photogalvanic effect was studied for the $Ru(bpy)_3^{2+}$–benzenethiolate anion system. The illuminated electrode showed a negative potential against the dark one. The photocurrent was proportional to both light intensity and concentration of $Ru(bpy)_3^{2+}$, and the action spectrum coincided with the electronic absorption spectrum of $Ru(bpy)_3^{2+}$. The current generation mechanism was in agreement with the kinetic mechanism proposed for the previous flash photolysis study. The photogalvanic effect in this system is attributable to the formation of $Ru(bpy)_3^{+}$ from the electron transfer quenching of $Ru(bpy)_3^{2+*}$ by benzenethiolate anion.

Introduction

Many photogalvanic cells based on photoinduced redox reactions have been investigated as photodevices for solar energy conversion.[1-8] A thionine–ferrous redox system has been extensively studied,[2-6] and the photocurrent was explained by the photostationary compositions of the il-

(1) Copeland, A. W.; Black, O. D.; Garrett, A. B. *Chem. Rev.* **1942**, *31*, 177.
(2) Rabinowitch, E. *J. Chem. Phys.* **1940**, *8*, 551, 560.
(3) Eisenberg, M.; Silverman, H. P. *Electrochim. Acta* **1961**, *5*, 1.
(4) Clark, W. D. K.; Eckert, J. A. *Sol. Energy* **1975**, *17*, 147.
(5) Gomer, R. *Electrochim. Acta* **1975**, *20*, 13.
(6) Wildes, P. D.; Lichtin, N. N. *J. Am. Chem. Soc.* **1978**, *100*, 6568.
(7) Kaneko, M.; Yamada, A. *J. Phys. Chem.* **1977**, *81*, 1213.

0022-3654/81/2085-3122$01.25/0